Hyperspectral microscopy as a particle exposure assessment tool

Carolina Blanch-Perez del Notario*[a], Pieter Bertier[b], Murali Jayapala[a] and Andy Lambrechts[a]

[a]Imec, Kapeldreef 75, 3001, Leuven, Belgium; [b]Belgian Center for Occupational Hygiene, BeCOH, Brusselsesteenweg 46, 3000 Leuven, Belgium

ABSTRACT

Hyperspectral imaging combines the characteristics of computer vision and point spectroscopy by obtaining an image with both spatial and spectral information. Therefore, in combination with microscopy, it can increase material discrimination possibilities with respect to regular microscopy imaging. We explore this increased discrimination potential to assess exposure to particle contamination, since workplace exposure to specific particle materials poses well-known health hazards. In this respect, we are focusing on discriminating more health relevant particles such as silica in the respirable size fraction. For this purpose, a particle sampling protocol has been proposed and hyperspectral imaging in combination with transmission microscopy is used for particle material identification. We use a Snapscan visual near-infrared (VNIR) camera providing high spectral and spatial resolution in the 460-900 nm range, 150 spectral bands and up to 7 Mpixels of spatial resolution and high acquisition speed. The hyperspectral microscopy system has been tested for discrimination of fifteen different particle materials, such as silica, coal, dolomite, barite, or rutile, among others. The combined analysis of spatial and spectral information shows potential to accurately discriminate the 15 tested particle materials so far by means of a random forest classifier. In addition, a band relevance analysis is performed showing that only a few specific bands are needed to provide accurate discrimination of the tested materials. The hyperspectral hardware and method presented could lead to a faster exposure assessment than traditional techniques used for occupational exposure estimation.

Keywords: Hyperspectral, microscopy, respirable particles, silica

1. INTRODUCTION

Crystalline silica or quartz (SiO2) is the most widely occurring of all minerals and it is found in most rocks. In the dry form, fine crystalline silica constitutes a toxic hazard since its inhalation as airborne dust could give rise to silicosis. Silicosis is pulmonary fibrosis which is regarded as the most common and severe of all pneumoconiosis[1]. The risk of developing the disease depends on three factors: dust concentration in the atmosphere; the percentage of silica in the dust, and the duration of exposure. Silica is encountered during many industrial processes which use minerals e.g. construction, quarrying and mining, brick, tile and refractory manufacture, pottery and ceramic, sandblasting, glass manufacture[2]. Exposure to crystalline silica or quartz can also be linked to immune system related diseases[3]. Specifically, silica has been linked to many autoimmune diseases, like systemic sclerosis, rheumatoid arthritis, systemic lupus erythematosus, and ANCA-positive vasculitis, but also to immune-mediated diseases that are not currently considered as autoimmune disorders, like sarcoidosis[4]. For this reason, workers' exposure to silica particles is monitored by occupational hygienists. In this respect, hygienists focus on the fraction of respirable crystalline silica particles[5]. Unlike inhalable dust, respirable dust cannot be seen in normal lighting as it is smaller than 15 micrometers in size. Due to their extremely small size, respirable dust particles can stay airborne for a significant amount of time and are inhaled deep into the lungs, reaching the alveoli and causing significant lung damage. There are currently several standardized sampling and analysis techniques from environmental and occupational hygienists to assess the exposure to silica particles. Aerosol samples are typically collected on filter substrates by size selective cyclones or foams and analyzed for their crystalline silica content in the laboratory by X-Ray Diffraction (XRD) or Fourier Transform Infra-Red (FTIR).

*carolina.blanch@imec.be; www.imec.be

Three-Dimensional and Multidimensional Microscopy: Image Acquisition and Processing XXXI, edited by
Thomas G. Brown, Tony Wilson, Laura Waller, Proc. of SPIE Vol. 12848, 1284803
© 2024 SPIE · 1605-7422 · doi: 10.1117/12.3002829

The latter are also the only two methods that are standardized for that purpose[6]EN 4. XRD is a non-destructive technique that provides detailed information about the crystallographic structure, chemical composition, and physical properties of a material[7]. FTIR[8] identifies chemical bonds in a molecule by producing an infrared absorption or reflection spectrum. These spectra produce a distinctive molecular profile of the sample that can indicate the components present. Other methods are mostly used for research purposes. Scanning electron microscopy[9] (SEM) or laser diffraction are laboratory methods that are often used for determining the particle sizes of dust deposits in workplaces or powdery materials used in industrial production processes. These methods only give information on particle size, not composition. For measurement of particle sizes of aerosols at the workplace, optical particle sizers, aerodynamic particle sizers [RefAPS], condensation particle counters or aerosol mobility spectrometers[10]are used. Phase contrast microscopy (PCM) and SEM/TEM+EDS (Transmission Electron Microscopy with Energy-dispersive X-ray Spectroscopy) are standardized methods for identifying fibrous compounds in aerosols (ISO 8672:2014, ISO 10312:2019). SEM/TEM+EDS is also used in occupational hygiene projects for identification and elemental characterization on non-fibrous particulate matter, but it is a labor- and cost intensive method. XRD, FTIR, laser diffraction particle sizing, SEM/TEM and PCM are laboratory methods, which implies that samples taken in the field must be taken to the laboratory for measurement and thus also that results are not directly available to the occupational hygienist during the sampling campaigns. Typical turnaround times for these kinds of analyses are several weeks. The National Institute for Occupational Safety and Health (NIOSH) has developed an FTIR method for analyzing the respirable crystalline silica content of aerosol samples collected on filter substrates at the workplace by means of a portable FTIR spectrometer and a purpose designed software[11]. This method offers the substantial advantage of providing the exposure data immediately after sampling ('end-of-shift' measurement). Yet, it requires an extensive database of measurement data from laboratory methods to deal with spectral interferences from other minerals. That data is available for the coal mining industry, for which the method was initially developed, but not for other industries.

This paper presents the use of Hyperspectral Imaging Systems (HSI) in combination with microscopy for the identification of hazardous substances in workplace dust samples. Hyperspectral imaging combines the characteristics of computer vision and point spectroscopy by obtaining an image with both spatial and spectral information. This technique enables therefore to analyze the chemical composition of materials while visualizing their spatial distribution[12], with its key advantages being that it is a non-invasive, non-contact and non-destructive technology. Hyperspectral imaging is comparable to FT-IR in the sense that both methods can be used to obtain reflectance or transmittance spectra in IR of the dust deposits. The key differences lie in the instrumentation used to collect these spectra, and their limitations with respect to time, area coverage, and spectral range. In FT-IR spectroscopy each measurement produces a spectrum from a single point, therefore inspecting a wider area is more time consuming. Hyperspectral imaging, instead, produces spectra of a full image and it can therefore cover larger areas in less time compared to FT-IR instruments. This can be done in a matter of a few minutes for linescan systems[13] down to less than a second in the case of the multispectral snapshot camera systems[14]. In addition, FT-IR imaging systems are highly complex and expensive with costs in the range of 200 k€[15]. The spectral range of HSI and FT-IR also differ. FT-IR spectra often cover the range of 400–4000 cm^{-1} equivalent to wavelengths of 2500–25,000 nm. HSI focuses on a smaller range of wavelengths, typically visible light (400–700 nm) and the near infrared region from 700 nm up to 2500 nm. HSI spectra have a narrower spectral range, but imaging large areas can be done in a much faster way than for FT-IR. In fact, there are many applications where hyperspectral imaging has gained high interest in the recent years: namely remote sensing, food inspection, medical surgery and diagnosis and industrial applications[16]. For instance, in ore, mineral and oil gas industries where hyperspectral core logging is becoming a routine process[37]. This growing interest has been partly fueled by technological advances in hyperspectral instrumentation. Hyperspectral cameras of lower size and cost factor providing faster acquisition and increased resolution have become available in the last decade[17].

There is a considerable amount of research dedicated to microplastic particle detection with hyperspectral imaging, mostly focusing on particle sizes over 500 µm. This way, four types of microplastics (PP, PE, PS and EPS pellets) have been imaged in the SWIR range (1000-2500 nm) and discriminated from organic material[18]. Similarly, pellets over 1mm of similar materials (PP, PE, PET, and PS) and other debris have been imaged in the SWIR range (1000-2500 nm) achieving accurate discrimination[19]. The same authors[20] have showcased hyperspectral imaging in the SWIR range as a high potential technology to analyze microplastics (< 5 mm), especially when compared to more expensive and time-consuming techniques such as Raman and FT-IR. The authors indicate however that insufficient spatial resolution is a current limitation in hyperspectral imaging to address smaller microplastics. Hyperspectral imaging has also received high interest as a method to discriminate different mineral types. Some authors have used hyperspectral imaging in the VNIR range (400-1000 nm) in combination with deep learning to identify minerals such as hematite, galena, and chalcopyrite in an ore[21]. Different hematite grain sizes are considered, from below 20 µm up to 1 cm and classification accuracies around 90% are obtained, in comparison with 30% for color imaging. Similarly, hyperspectral imaging in the LWIR range (7.7 to 11.8 µm) has been used to accurately discriminate 21 different mineral powders and 3 mixes of them[22]. Among these, materials such as silica and muscovite are present. The impact of grain size distribution is considered, with ranges from about means of 12 µm up to around 600 µm of grain size. Both SWIR (1000-2500 nm) and LWIR (7.5 to 11.5 µm) imaging have been evaluated for detection of clay minerals in sand[23]. Prediction of quartz and clay contents could be accurately done and compared with more expensive and time-consuming reference methods such as x-ray fluorescence spectroscopy (XRF) or x-ray diffraction (XRD). However, all this work focuses on inspection of bulk mineral samples or particle aggregations and does not address single particle inspection. Single particle inspection requires the combination of microscopy and hyperspectral imaging. In this context, dark field hyperspectral microscopy has been used in the 400-1000 nm range to detect nano particles in biological tissues[24]. While optical microscopy is not able to detect nanoscale particles (< 200 nm) due to its diffraction-limited resolution, dark field microscopy overcomes this diffraction limit and offers a faster, effective, and cheaper alternative than other expensive techniques such as electron microscopy to image nanoparticles. Finally, a high-throughput spectroscopy and microscopy imaging system has been proposed for characterization of gold nano particles at the single-particle level[25], enabling a single snapshot image of 1024x1024 pixels at high temporal resolution (26 fps) in the visual spectral range of 400-700 nm. The developed method enables quantification of spectra and spatial information. However, only gold nanoparticle detection is addressed. Only this last work[25] shows different material discrimination of 2 or 3 different material types. Our work also focuses on individual mineral particle discrimination but for bright-field imaging. In our case we target particles of respirable size (~ 5 µm) and address discrimination of up to 15 different material types, with focus on health-relevant particles such as silica. Moreover, a band relevance analysis is performed to identify the subset of a few required spectral bands from the original set of 150 bands in the 470-900 nm range. The purpose of the work done is to explore the potential of hyperspectral microscopy as an alternative method to discriminate particle materials. This technology would then allow a first fast assessment of the worksite exposure by means of a portable hyperspectral system. In this respect, the already available compact hyperspectral cameras[13, 14] are expected to pave the way for a cost-effective on-site exposure inspection system.

2. MATERIALS AND METHODS

2.1 Particle samples and sampling protocol

For the selection and preparation of relevant particle materials, health-relevant materials like silica are included, together with potential confounders particles that can be present simultaneously (e.g barite). By confounder we mean particles that could be present in the same sampling environment and be similar enough to be mistaken/misclassified by a target health-relevant material such as silica particles. A set of 15 different material particle powders was prepared including quartz (the most common polymorph of crystalline silica). The particle types and its grain-size distribution are shown in Table 5, with a mean particle size in the order of 5 µm. The focus is to detect and discriminate health relevant particles, such as silica, and specifically those at respirable size (below 15 microns), since those can penetrate beyond the terminal bronchioles into the gas-exchange region of the lungs and may propagate via blood to other organs in the body. The powder characterization method used for these samples was bulk X-ray diffraction (XRD) for mineralogy analysis and grain-size analysis by laser diffraction. The samples were additionally tested for purity. These particle samples were then deposited onto glass slides to have samples suitable for hyperspectral microscopy imaging.

Table 1: Statistical parameters of the grain-size distribution of the sample (in µm).

Parameter	**Calcite**	**Carbon**	**Dolomite**	**Gibbsite**	**Gypsum**	**Hematite**	**Kaolinite**	**Barite**
Mean (µm)	4.80	6.36	3.44	6.72	3.80	3.99	4.82	6.49
Standard dev	4.34	5.18	2.66	4.83	2.25	2.93	3.34	5.99
Mode (µm)	3.23	5.52	3.36	4.87	3.50	3.23	3.81	12.62
Skewness	2.37	1.49	2.56	1.42	1.20	1.60	1.55	1.98
Kurtosis	15.83	2.50	833.1	2.07	1.75	3.14	2.77	360.94
d10(µm)	1.38	1.40	0.66	2.11	1.46	1.21	1.65	0.83
d50(µm)	3.44	4.85	2.82	5.27	3.30	3.16	3.86	4.20
d90(µm)	9.98	13.58	7.05	13.65	6.86	7.98	9.41	15.54
Parameter	**Feldspar**	**Muscovite**	**Phlogopite**	**Quartz**	**Rutile**	**Smectite**	**K-spar**	**Goethite**
Mean (µm)	5.03	0.42	3.39	3.78	0.31	1.59	5.01	13.00
Standard dev	3.53	0.30	2.32	2.12	0.54	1.06	3.19	10.72
Mode (µm)	3.97	0.38	3.10	3.50	0.26	1.67	4.31	20.37
Skewness	1.66	2667.57	10.74	1.19	3779.15	27.71	1.41	1.30
Kurtosis	3.43	390.02	873.21	1.59	1989.67	487.65	2.36	126.08
d10(µm)	1.73	0.18	1.04	1.54	0.16	0.42	1.84	0.77
d50(µm)	4.03	0.37	2.87	3.30	0.28	1.37	4.19	10.96
d90(µm)	9.77	0.74	6.52	6.72	0.51	3.07	9.38	28.42

A particle sampling protocol has been established to obtain samples suitable for microscopy inspection in combination with hyperspectral imaging. This sampling protocol is meant to be as well a pragmatical and simple approach to test for particle exposure onsite. The goal is to sample particles that may be present in dust deposits covering surfaces at workplaces. For this purpose, we first performed a few tests to evaluate the impact of different types of tapes set on a microscopy glass slide. Different tapes may have different adhesive properties and may as well impact the acquired spectral signature in a different way. Regular microscopy glass slides[26] have been used since they are very suitable for imaging with a transmission microscope. We evaluated here the potential risk of spectral interference of the glass material (being silica) with the discrimination of silica particles. We tested two types of tapes, tesa double-side tape[27] and single tape[28]. Better adhesive properties were observed in the tesa double-side tape of the particles to the tape and the tape to the glass slide. Therefore, the tesa tape was selected since this helped achieve good focus and better image quality. In this respect, both glass slide and transparent tape will contribute to the measured spectra of transparent particles such as silica.

2.2 Hyperspectral microscopy system

The imaging system used is depicted in Figure 1, a Snapscan camera[13], which offers both high spatial resolution (up to 3650 x 2048px, 7Mpixels) and high spectral resolution (150 bands) over the wavelength range of 460 to 900 nm. This camera is coupled to a Leica transmission microscope[29] and performs the scanning internally. Thanks to its internal translation stage, there is no need for an external scanning movement. Scanning is handled internally, performing data-set acquisition as easily as with a snapshot camera and full hyperspectral images can be acquired in less than 1 minute. A 20x magnification objective is used in combination with bright field imaging. The microscope has a broadband tungsten-halogen light source, covering the 460-900 nm range of our hyperspectral camera.

The set of 15 particle samples at respirable sizes are placed on glass slides according to the protocol described previously and imaged with the Snapscan VNIR in combination with the transmission microscope and a magnification objective of 20x.

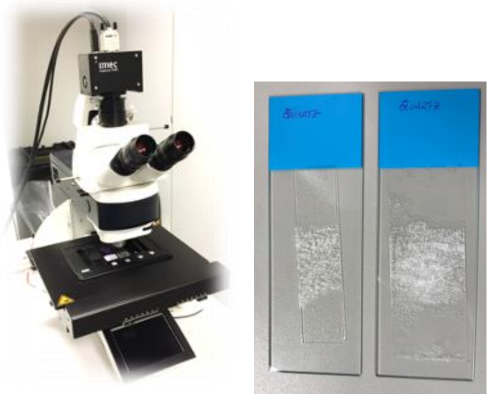

Figure 1: Hypesrpectral microscopy system (left) and example of prepared glass slides with particle samples.

2.3 Hyperspectral processing pipeline

The high pixel spectral variation within each particle makes it more challenging to attain high accuracy in material classification. Therefore, to deal with this spectral variability and to increase the classification performance, spectral means of a group of pixels within each particle were used. Pixel mean values ranging from 10-pixel to 1000-pixel means were tested and a final value of 100-pixel means was selected. To extract the pixel means within each particle, segmentation of particles from the background was required. As a first approach, a manual particle segmentation is implemented to be able to show the proof of concept of particle discrimination based on its spectra. However, it has been explored how to later automate this segmentation with the "Superpixel" function available in Matlab[30]. This function groups neighboring pixels according to its similarity and builds the so-called super pixels. The expectation is then that those super pixels either belong to the background or to one single particle, which then allows us to obtain spectral means within each particle. The prior required step is to segment background from particles in the image. This can be done by thresholding a selected high-contrast band image (in our case band 67, corresponding to 660.46 nm). The threshold value of 0.65 is found to be a good selection to obtain a clear segmentation in all images. This provides an image with '0' value at the background pixels (shown as black) and '1' value at the particle pixels (shown as white). Segmentation generally succeeds in separating particles and background well, although occasionally the center of big particles can present an area misclassified as background. In this case, morphological operations on an image [30,31] can help close those small gaps. The next step after background-particle segmentation is to partition the image into super-pixels (neighboring areas of close similarity). By choosing the required number of super-pixels per image we can obtain super-pixels with varying size of pixels (for instance in the range of 100 to 1000 pixels). Alternatively, to obtain the approximate desired 100-pixel means, groups of 100 pixels from the bigger super-pixel can be selected. In practice, however, using a bigger group that 100 pixels to extract the spectral means is also a possibility since it provides similar performance. Figure 2 shows the general processing pipeline implemented.

The classifiers are implemented with PerClass software[32] in combination with Matlab processing software[30]. All of these are pixel-based classifiers; therefore, no spatial information is used to support classification. The classifiers under consideration are:

- Linear Discriminant Classifier (LDC) [33]
- Quadratic Discriminant Classifier (QDC) [33]
- Random Forest (RF) [32]

While the preprocessing steps considered are either none or:

- Linear Discriminant Analysis (LDA) [33]
- Median Filtering[34] (MF) over a 3x3 or 5x5 block of surrounding pixels.
- Means of particle spectra, as previously explained.

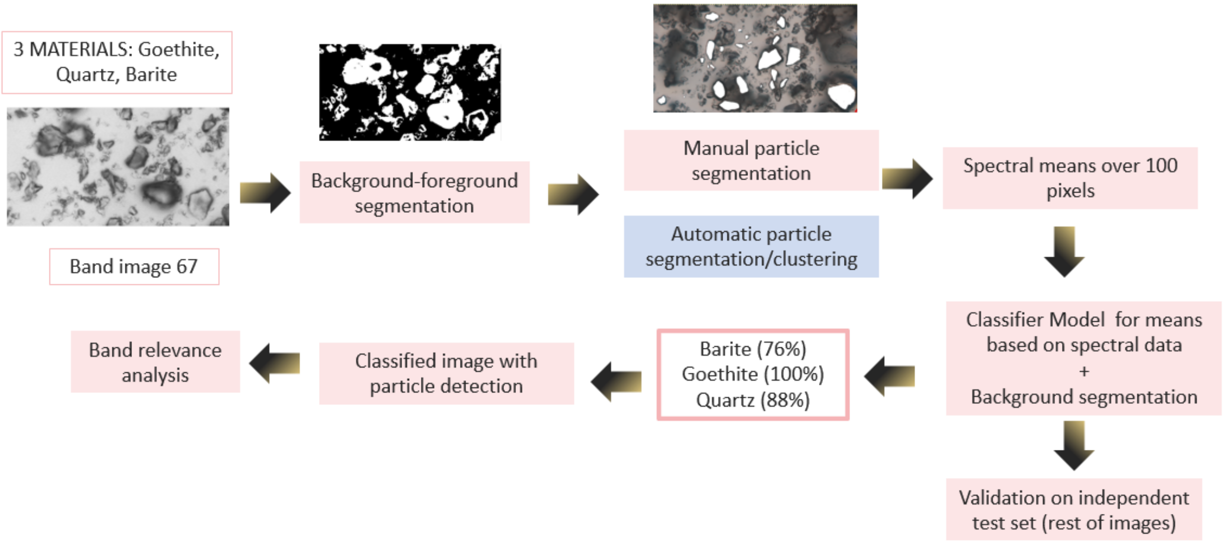

Figure 2: Processing pipeline for discrimination of 3 particle materials

To find the most discriminative bands in our wavelength range, an in-house developed Genetic Algorithm[35,36] in combination with the pixel classifier is used. The algorithm aim is to find a near-optimal subset of bands providing the highest mean classification accuracy in the test set.

The behavior of the Genetic Algorithm is summarized here and in Figure 3:

- For a desired number of subset bands/wavelengths (e.g 3...) an initial 'population' of individuals is created. Every 'individual' consists of a specific set of random band selections (e.g. [630nm, 770nm, 900nm]. An individual with a uniform selection is also included in the initial population.
- For each individual solution (band selection) the fitness function of the Genetic Algorithm is computed as the mean classification accuracy obtained for that band subset on a fixed training and testing set.
- The Genetic Algorithm iterates for a given number of iterations the best 'individual' or band subset is kept.

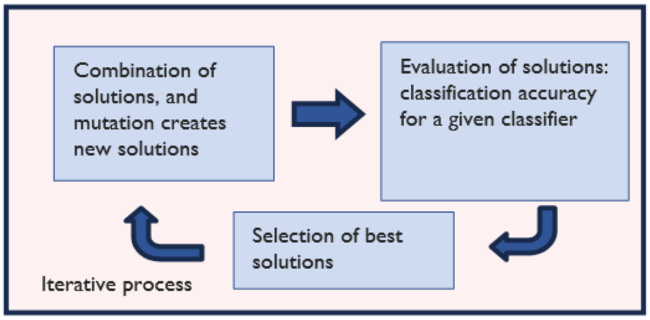

Figure 3: Schematics of Genetic Algorithm

3. RESULTS AND DISCUSSIONS

The mean reflectance spectra of the particle materials considered is shown in Figure 4. Despite the fact that the materials' spectra in this range does not have too prominent absorption bands, the experimental results show that this spectral information is discriminative enough.

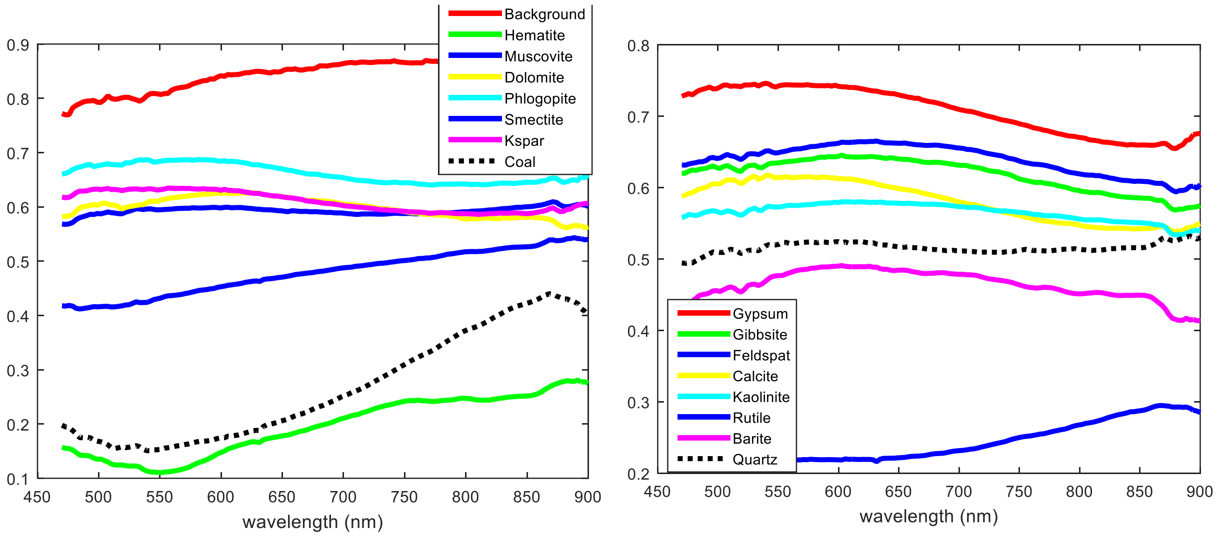

Figure 4: Mean reflectance spectra of the different particle materials in the Snapscan VNIR range (460-900 nm)

Several pixel-based classifiers are tested in combination with different preprocessing steps. All these pixel classifiers are compared for a distribution of 30% pixel means for training and 70% pixel means for the testing set. The following Table compares several pixel-based classifiers showing its mean performance (averaged over the 15 materials) but also the maximum/highest accuracy obtained per material and the minimum/lowest accuracy per material. The use of a Random Forest (RF) classifier increases the mean performance considerably from 69% (LDA+QDC) to 93% (RF). With QDC classifier, 5 materials obtain too low pixel mean accuracy (below 50%) for their particles to be correctly recovered. With RF even the materials with lowest accuracy reach 83%-pixel accuracy, which guarantees the correct classification of the full particle by using majority vote.

Table 2: Pixel classification accuracy for different classifiers, 100-pixel means and 15 different materials.

Classifier	Mean accuracy	Max accuracy	Minimum accuracy
LDA+QDC	69.3%	97%	12% (5<50%)
RF	93.0%	100%	83%
LDA+RF	90.5%	99%	78%

The following Figure 5 shows the confusion matrix for LDA as preprocessing step and Random Forest as classifier. The numbers in the diagonal of the confusion matrix represent how accurately (between 0 and 1) each pixel material type is classified as such. Values outside of the diagonal correspond to pixel miss-classifications between the true labels (known material) and the decision taken by the classifier (assigned material during classification). Therefore, the higher the values in the diagonal (close to 1) and the lower the value outside the diagonal means very accurate classification with few pixel material miss-classifications. The classification accuracy achieved for all material types is very high, ranging from 78% for dolomite and phlogopite to 99% accuracy for barite. Additionally, the misclassifications are very low, with typically only 1-4% of the pixels that are misclassified from one to another category.

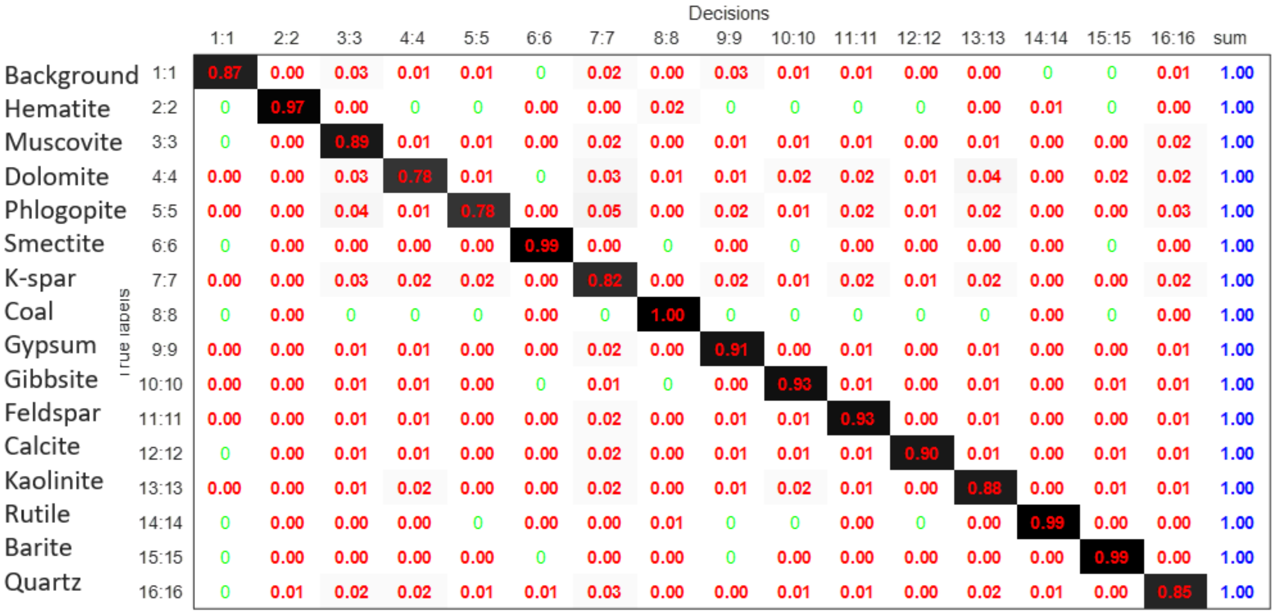

Decisions

	True labels	1:1	2:2	3:3	4:4	5:5	6:6	7:7	8:8	9:9	10:10	11:11	12:12	13:13	14:14	15:15	16:16	sum
Background	1:1	0.87	0.00	0.03	0.01	0.01	0	0.02	0.00	0.03	0.01	0.01	0.00	0.00	0	0	0.01	1.00
Hematite	2:2	0	0.97	0.00	0	0	0.00	0.00	0.02	0	0	0	0	0.00	0.01	0	0.00	1.00
Muscovite	3:3	0	0.00	0.89	0.01	0.01	0.00	0.02	0.00	0.01	0.01	0.01	0.00	0.01	0.00	0.00	0.02	1.00
Dolomite	4:4	0.00	0.00	0.03	0.78	0.01	0	0.03	0.01	0.01	0.02	0.02	0.01	0.04	0.00	0.02	0.02	1.00
Phlogopite	5:5	0.00	0.00	0.04	0.01	0.78	0.00	0.05	0.00	0.02	0.01	0.02	0.01	0.02	0.00	0.00	0.03	1.00
Smectite	6:6	0	0.00	0.00	0.00	0.00	0.99	0.00	0	0.00	0	0.00	0.00	0.00	0.00	0	0.00	1.00
K-spar	7:7	0.00	0.00	0.03	0.02	0.02	0.00	0.82	0.00	0.02	0.01	0.02	0.01	0.02	0.00	0.00	0.02	1.00
Coal	8:8	0	0.00	0	0	0	0.00	0	1.00	0	0	0	0	0	0.00	0	0.00	1.00
Gypsum	9:9	0.00	0.00	0.01	0.01	0.00	0.00	0.02	0.00	0.91	0.00	0.01	0.00	0.01	0.00	0.00	0.01	1.00
Gibbsite	10:10	0.00	0.00	0.01	0.01	0.00	0	0.01	0	0.00	0.93	0.01	0.00	0.01	0.00	0.01	0.01	1.00
Feldspar	11:11	0.00	0.00	0.01	0.01	0.00	0.00	0.02	0.00	0.01	0.01	0.93	0.00	0.01	0.00	0.00	0.01	1.00
Calcite	12:12	0	0.00	0.01	0.01	0.00	0.00	0.02	0.00	0.01	0.01	0.01	0.90	0.01	0.00	0.01	0.01	1.00
Kaolinite	13:13	0.00	0.00	0.01	0.02	0.00	0.00	0.02	0.00	0.01	0.02	0.01	0.00	0.88	0.00	0.01	0.01	1.00
Rutile	14:14	0	0.00	0.00	0.00	0	0.00	0.00	0.01	0	0	0.00	0	0.00	0.99	0.00	0.00	1.00
Barite	15:15	0	0.00	0.00	0.00	0.00	0	0.00	0.00	0	0.00	0.00	0.00	0.00	0.00	0.99	0.00	1.00
Quartz	16:16	0	0.01	0.02	0.02	0.01	0.01	0.03	0.00	0.00	0.01	0.01	0.00	0.02	0.01	0.00	0.85	1.00

Figure 5: Confussion matrix for LDA+Random Forest classifier on the Snapscan VNIR spectra

Note that at object level (particle level) a pixel majority vote can be used to determine the resulting material label of a full particle. Therefore, a 78% accurate pixel classification would translate into noticeably higher classification accuracy at particle level. To visualize this, Figure 6 shows a close-up of the classified images with the color label attached for some selected particles. The rest of the particles are not considered in the classification, only a few highlighted particles are manually selected to show the feasibility of spectral discrimination. The resulting classified images show how the high classification accuracy translates into correct color labeling/classification for the selected particles.

The analysis performed shows that, based on the Snapscan spectra of 150 bands, high classification accuracy of these 15 different materials is obtained. However, in practice, there is a lot of redundancy between consecutive narrow bands and a much lower number of bands may be required to achieve accurate classification. Moreover, requiring a lower number of spectral bands can reduce memory and processing requirements and enable the future use of lower resolution snapshot cameras[14] with fewer spectral bands. These compact snapshot cameras provide the additional advantage of a high acquisition speed (up to 180 fps).
Table 3 shows the most relevant bands extracted from the Genetic Algorithm and the initial set of 150 bands. The classification accuracies provided, for the best performing classifier (RF), refer again to pixel accuracies, therefore with majority-vote at object level an even higher accuracy is obtained. The band relevance analysis performed shows that only a few narrow wavelengths may be required to discriminate the materials considered. For instance, restricting the number of bands to the best 9 provides almost the same accuracy as using all 150 bands. Similarly, with the best 5 band selection a high accuracy is reached for all materials of at least 75%. Only when reducing to 3 or 2 bands, the performance degradation becomes more noticeable.

Table 3: Mean/Max/Min classification accuracies for different band subsets.

# of Bands	Bands (nm)	Mean	Max	Min
All 150	460 … 900 nm	92.97%	99%	83%
Best 9	470 472.8 513 726.8 816.3 850.9 874 879.8	90.69%	99%	77%
Best 5	484.4 562.2 640.2 850.9 885.5	90.49%	99%	75%
Best 3	643.1 718.1 871.1	90.3%	99%	71%

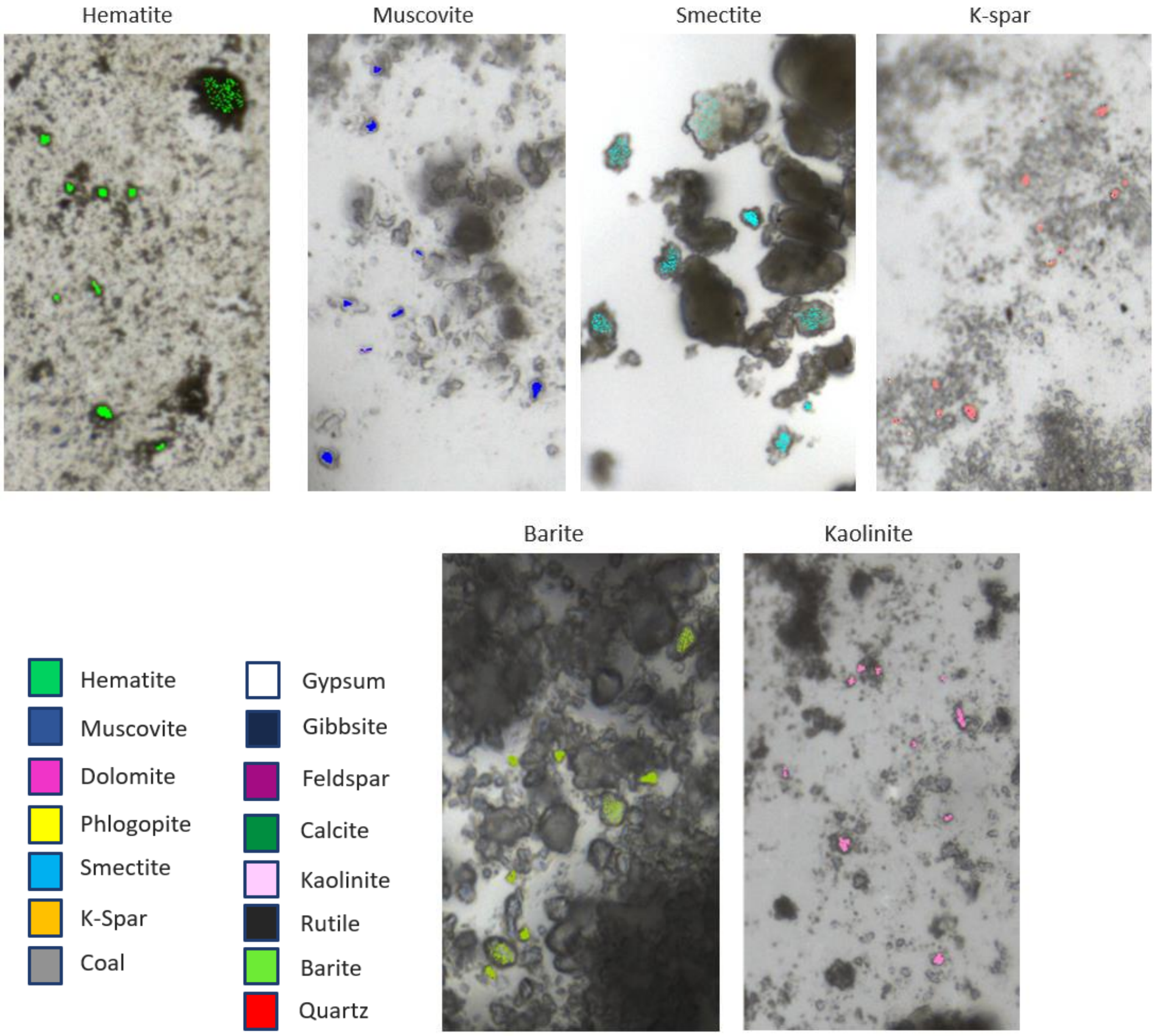

Figure 6: Close-up of classified images for selected particles of six different samples of particle materials.

4. CONCLUSION

This paper has explored the potential of hyperspectral imaging in combination with microscopy with the purpose of particle material discrimination. The goal is to develop a method for a first fast assessment of the particle materials present at a worksite by means of using a cost-effective hyperspectral system. The focus has been on identification of respirable size particles (around 5 µm), which are health relevant such as silica, and to discriminate them from other particle materials that may be present simultaneously. A sampling protocol has been developed by using tape and a glass slide, to enable sample inspection with a transmission microscope coupled to a hyperspectral camera. The results show that by averaging over particle pixels high classification accuracies (over 90%) can be obtained with a Random Forest classifier. A band relevance analysis of the high-resolution hyperspectral camera with 150 bands has shown that a few bands (<10) in the visual near-infrared range are sufficient to still achieve high classification accuracy. Therefore, future work could involve the testing of lower resolution (16-25 spectral bands) snapshot cameras, since these could be sufficient for accurate discrimination of particle materials while enabling faster acquisition.

ACKNOWLEDGEMENTS

We want to acknowledge the Eximious project, for which this research has been done. This project has received funding from the European Union's Horizon 2020 research and innovation programme under grant agreement No 874707. We also want to thank Rieko Adriaens for his powder sample preparation and our colleague Bart Aerts for his help in the particle sample preparation suitable for hyperspectral imaging.

REFERENCES

[1] Mlika M, Adigun R, Bhutta BS. Silica-Induced Pneumoconiosis. 2023 Feb 9. In: StatPearls [Internet]. Treasure Island (FL): StatPearls Publishing; 2023 Jan–. PMID: 30726026.
[2] Occupational Hygiene Training Association (OHTA) Student Manual. From https://aiha-assets.sfo2.digitaloceanspaces.com/AIHA/ohta-uploads/Training-Docs/W201-Basic-Principles/KA02-v3-1-31Jul19-Student-Manual-English.pdf
[3] Miller et al, 2012, J Autoimmune 39: 259–71; Parks et al, 2014, Int J Mol Sci 15: 14269–97.
[4] Mapping Exposure-Induced Immune Effects: Connecting the Exposome and the Immunome | EXIMIOUS Project | Fact Sheet | H2020 | CORDIS | European Commission n.d. https://cordis.europa.eu/project/id/874707 (accessed July 7, 2022).
[5] "Health based particle-size-selective sampling", Application Note ITI-050. Available at https://tsi.com/getmedia/c388c1e7-9ab4-4f88-9f76-f2a3b64ba293/ITI-050?ext=.pdf
[6] ISO 16258, EN 17289 "Characterization of bulk materials – Determination of a size-weighted fine fraction and crystalline silica content – Part 1: General information and choice of tests methods", European Standard EN 17289-1.https://standards.iteh.ai/catalog/standards/cen/7d2afbcc-5913-402c-88e2-0dc4e9046681/en-17289-1-2020
[7] ISO 16258:2015 - Workplace air - Analysis of respirable crystalline silica by X-ray diffraction
[8] ISO 19087:2018 - Workplace air — Analysis of respirable crystalline silica by Fourier-Transform Infrared spectroscopy
[9] Wijnand Eduard, Stephan Weinbruch, Asbjørn Skogstad, Øivind Skare, Karl-Christian Nordby, Hilde Notø, Content of clinker and other materials in personal thoracic aerosol samples from cement plants estimated by scanning electron microscopy and energy-dispersive X-ray microanalysis, *Annals of Work Exposures and Health*, Volume 67, Issue 8, October 2023, Pages 990–1003, https://doi.org/10.1093/annweh/wxad047
[10] Evanly Vo, Matthew Horvatin, Ziqing Zhuang, Performance Comparison of Field Portable Instruments to the Scanning Mobility Particle Sizer Using Monodispersed and Polydispersed Sodium Chloride Aerosols, *Annals of Work Exposures and Health*, Volume 62, Issue 6, July 2018, Pages 711–720, https://doi.org/10.1093/annweh/wxy036
[11] Taekhee Lee, Larry Lee, Emanuele Cauda, Jon Hummer and Martin Harper, "Respirable size-selective sampler for end-of-shift quartz measurement: Development and performance", in Journal of Occupational and Environmental Hygiene, vol 14, 5, pp 335-342, 2017. https://doi.org/10.1080/15459624.2016.1252845
[12] Kamruzzaman M., El Masry G., Sun D-W. & Allen P. (2012) "Non-destructive prediction and visualization of chemical composition in lamb meat using NIR hyperspectral imaging and multivariate regression". Innovative Food Science and Emerging Technologies vol 16 (2012), pp 218-226.
[13] Pichette, J., Charle, W., & Lambrechts, A. Fast and compact internal scanning CMOS-based hyperspectral camera: the Snapscan. In Photonic Instrumentation Engineering IV (Vol. 10110, p. 1011014). International Society for Optics and Photonics, (2017).
[14] Geelen, B., Blanch, C., Gonzalez, P., Tack, N., & Lambrechts, A. (2015). A tiny VIS-NIR snapshot multispectral camera. In Advanced Fabrication Technologies for Micro/Nano Optics and Photonics VIII (Vol. 9374, p. 937414). International Society for Optics and Photonics, March 2015.
[15] Primpke S, Christiansen SH, Cowger W, De Frond H, Deshpande A, Fischer M, et al. Critical Assessment of Analytical Methods for the Harmonized and Cost-Efficient Analysis of Microplastics. Appl Spectrosc. 2020; 74(9):1012–47. https://doi.org/10.1177/0003702820921465

[16] Khan, M. J., Khan, H.S, Yousaf, A., Khurshid, K. & Abbas, A. (2018). “Modern trends in hyperspectral image analysis: a review”. IEEE Access Open Access Journal, Digital Object Identifier 10.1109/ACCESS.2018.2812999, March 2018.

[17] West, M., Grossmann, J., & Galvan, C. (2019). “Commercial Snapshot Spectral Imaging: The Art of the Possible.”

[18] Serranti, S., Fiore, L., Bonifazi, G., Takeshima, A., Takeuchi, H., & Kashiwada, S. (2019, November). Microplastics characterization by hyperspectral imaging in the SWIR range. In SPIE Future Sensing Technologies (Vol. 11197, pp. 134-140). SPIE.

[19] A. Faltynkova, M. Wagner, “Developing and testing a workflow to identify microplastics using near infrared hyperspectral imaging”, Chemosphere, Volume 336, 2023, 139186, ISSN 0045-6535, https://doi.org/10.1016/j.chemosphere.2023.139186.

[20] Faltynkova, A., Johnsen, G. & Wagner, M. “Hyperspectral imaging as an emerging tool to analyze microplastics: A systematic review and recommendations for future development”. Micropl.&Nanopl. 1, 13 (2021). https://doi.org/10.1186/s43591-021-00014-y

[21] Okada, N., Maekawa, Y., Owada, N., Haga, K., Shibayama, A., & Kawamura, Y. (2020). Automated identification of mineral types and grain size using hyperspectral imaging and deep learning for mineral processing. Minerals, 10(9), 809.

[22] Myers, T. L., Johnson, T. J., Gallagher, N. B., Bernacki, B. E., Beiswenger, T. N., Szecsody, J. E., ... & Danby, T. O. (2019). Hyperspectral imaging of minerals in the longwave infrared: the use of laboratory directional-hemispherical reference measurements for field exploration data. Journal of Applied Remote Sensing, 13(3), 034527-034527.

[23] Entezari, I., Rivard, B., Geramian, M., & Lipsett, M. G. (2017). Predicting the abundance of clays and quartz in oil sands using hyperspectral measurements. International journal of applied earth observation and geoinformation, 59, 1-8.

[24] R. Fakhrullin, L.Nigamatzyanova, G. Fakhrullina, “Dark-field/hyperspectral microscopy for detecting nanoscale particles”. In environmental nanotoxicology research, Science of The Total Environment, Volume 772, 2021, 145478, ISSN 0048-9697, https://doi.org/10.1016/j.scitotenv.2021.145478.

[25] J. E. Batey, M. Yang, H. Giang, and B. Dong, “Ultrahigh-Throughput Single-Particle Hyperspectral Imaging of Gold Nanoparticles”, in Analytical Chemistry, vol 95, 13. 2023. https://doi.org/10.1021/acs.analchem.2c05336.

[26] Microscope slides ground color frosted blue (ECN 631-1562)

[27] Tesa 64621-00000-04 Double-sided adhesive tape, transparent, 10m:12mm

[28] Scotch single-sided Crystal tape, 19 mm

[29] https://www.manualslib.com/products/Leica-Dm5000b-3043767.html

[30] Matlab (2019). The Mathworks, Natick. https://mathworks.com.

[31] Bhutada, S, Yashwanth et al. Opening and closing in morphological image processing. In World Journal of Advanced Research and Reviews, 2022, 14(03), 687–695. June 2022 https://doi.org/10.30574/wjarr.2022.14.3.0576

[32] PerClass BV 2008-2022, Delft, NL. http://perclass.com/perclass-toolbox/product

[33] Naes, T., Isaksson, T., Fearn, T. & Davies, T. “A User-Friendly Guide to Multivariate Calibration and Classification”. NIR Publications (2004).

[34] Gonzalez, R.C & Woods, R.E “Digital Image Processing”, Eaglewood Cliffs, NJ: Prentice-Hall, 2002.

[35] Holland, J. H. (1992). Genetic algorithms. Scientific American, 267. https://doi.org/10.1038/scientificamerican0792-66.

[36] Blanch-Perez-del-Notario, C., Baert, R., & D'Hondt, M. (2012). Multi-objective genetic algorithm for task assignment on heterogeneous nodes. International Journal of Digital Multimedia Broadcasting, 2012, 1-12.

[37] Teledyne DALSA. (2023, April 25). Hyperspectral Imaging in Oil, Mineral and Environmental Industries. AZoOptics. Retrieved on January 10, 2024 from https://www.azooptics.com/Article.aspx?ArticleID=1305.